Mass yield features of (γ,π^+) and $(\gamma,\pi^- xn)$ reactions for $x=0-9$ on complex nuclei in the Δ region

Koh Sakamoto, Samir Ranjan Sarkar, Yasuji Oura, Hiromitsu Haba, Hiroshi Matsumura, and Yutaka Miyamoto
Department of Chemistry, Faculty of Science, Kanazawa University, Kanazawa, Ishikawa 920-1192, Japan

Seiichi Shibata
Research Reactor Institute, Kyoto University, Sennan-gun, Osaka 590-0494, Japan

Michiaki Furukawa
Faculty of Environmental and Information Sciences, Yokkaichi University, Yokkaichi, Mie 512-8512, Japan

Ichiro Fujiwara
School of Economics, Otemon Gakuin University, Ibaraki, Osaka 567-8502, Japan
(Received 26 October 1998)

Radiochemical measurements of the product yields from (γ,π^+) and $(\gamma,\pi^- xn)$ reactions for $x=0-9$ were performed on targets of ^{27}Al, ^{37}Cl, ^{41}K, ^{51}V, ^{59}Co, ^{65}Cu, ^{75}As, ^{87}Rb, ^{88}Sr, ^{109}Ag, ^{115}In, ^{133}Cs, ^{138}Ba, ^{139}La, and ^{181}Ta, and of ^{7}Li, ^{11}B, ^{14}N, ^{44}Ca, ^{51}V, ^{56}Fe, ^{59}Co, ^{63}Cu, ^{65}Cu, ^{75}As, ^{88}Sr, ^{89}Y, ^{109}Ag, ^{115}In, ^{127}I, ^{130}Te, ^{133}Cs, ^{139}La, ^{175}Lu, ^{197}Au, and ^{209}Bi, respectively, over bremsstrahlung end-point energies (E_0) of 30–1200 MeV in steps of $E_0=50$ MeV or less. Yield variations as a function of the number of the emitted neutrons (x) for each target at $E_0\geqslant 400$ MeV were found to be typical of (3,3) resonance. The reactions for neutron multiplicities as large as $x\geqslant 6$ are notable for targets of mass $A_t\geqslant 100$, while only the reactions for smaller x are measurable for the lighter targets. The yields for both (γ,π^-) and (γ,π^+) are A_t-independent for targets heavier than $A_t>30-40$, while much smaller yields are reported for targets with $A_t=7-14$. The yield ratio $(\gamma,\pi^-)/(\gamma,\pi^+)$ becomes as high as 5.5 and such a high value suggests that the neutron density in the surface region of nucleus is higher than that expected from the neutron-to-proton ratio for the entire nucleus. The observed yields for individual $(\gamma,\pi^- xn)$ reactions having equal x were also found to be a smoothly varying function of the neutron-to-proton ratio of the target, $(N/Z)_t$, not of the target mass, A_t or number of target neutrons, N_t. This implies that the reactions are initiated via competitive photoabsorptions by neutrons and protons in the target nucleus. The smooth variation of the profile changes its characteristics at $(N/Z)_t=1.30-1.40$, corresponding to $A_t=100-130$; this implies higher excitation energies due to progressively larger medium effects in nuclei with $A_t>100$. The results are compared with theoretical calculations made using the photon-induced intranuclear cascade and evaporation analysis program by Gabriel and Alsmiller.
[S0556-2813(99)05703-9]

PACS number(s): 25.20.Lj

I. INTRODUCTION

This paper reports our current results of radiochemical yield measurements for the photopion reactions of (γ,π^+) and $(\gamma,\pi^- xn)$ for $x=0-9$ for a wide range of complex target nuclei in the Δ formation region. In our previous paper [1], the mass yield features of ^{133}Cs$(\gamma,\pi^- xn)^{133-x}$Ba for $x=0$, 2, 4, 5, 6, 7, and 9 were compared with those of ^{51}V$(\gamma,\pi^- xn)^{51-x}$Cr for $x=0$, 2, and 3 [2]. The shape of the mass yield curve was quite different in the two targets. The yields for $^{133-x}$Ba from ^{133}Cs showed a broad maximum around $x=3$ for the relevant energies, indicating the excitation energy remaining in the target nucleus after π^- emission is sufficiently high to evaporate 7 to 9 neutrons with appreciable probabilities. The reaction yield for ^{51}Cr from ^{51}V(γ,π^-) is much higher than those for ^{49}Cr and ^{48}Cr from ^{51}V$(\gamma,\pi^- 2n)$ and ^{51}V$(\gamma,\pi^- 3n)$ in the same energy region. A further study on the yields of ^{127}I$(\gamma,\pi^- xn)^{127-x}$Xe for $x=0$, 2, 4, 5, and 6 [3] gave a mass yield pattern similar to that of $^{133-x}$Ba from ^{133}Cs, while the (γ,π^-) reaction yields were lower than those for reactions associated with multiple neutron emission and very similar for all three targets. The (γ,π^+) yields for ^{133}Cs, ^{87}Rb, ^{51}V, ^{41}K, and ^{27}Al targets were also found to be target-mass independent. A remarkable fact was that the yield ratios for (γ,π^-) to (γ,π^+) reactions on the studied targets are 5–6.

The yield curves for the individual reaction products as a function of the maximum end-point energy (E_0) of the bremsstrahlung beam, and the excitation functions as a function of the photon energy (k) obtained by unfolding of the yield curves were found to be characteristic of the Δ resonance, though affected by the nuclear medium, and indicated a smooth variation with respect to neutron multiplicity (x).

In the Δ formation region, an incoming photon interacts with a single nucleon inside the target nucleus to produce an excited nucleon (Δ) which decays immediately (10^{-24} sec) into a stable nucleon and a pion, and either one or both particles produced in this initial process may escape from the nucleus or develop a cascade-evaporation process in the same nucleus. The probability of the escape depends on the location of photoabsorption by the nucleon and the nuclear transparency of the associated particles. If the pion is emitted in a forward direction at a small angle, the nucleus is left

with insufficient energy for developing a cascade process. Most of the previous physical investigations were restricted to the inclusive measurements of one or two of the emitted particles, and ascribed the pion and/or nucleon emission(s) to simple reactions such as (γ,π^0), $(\gamma,\pi^{\pm})$, (γ,p), and (γ,n) on light nuclei. A series of double differential cross section measurements of pions and nucleons ($2p$ and pn) from heavier targets were reported [4], and the dependence of the energy-integrated differential cross sections on the nuclear size (S), S being the number of protons or neutrons in the target, was found to be described by $d\sigma/d\Omega \propto S^{\alpha}$, where the exponent is 0.6 for $\pi^{\pm}$ and 1.15 for a proton. The authors explained the results of the cross sections as a consequence of a combination of volume production and pion reabsorption, although pure surface production could not be excluded from the pion data [4]. These inclusive measurements did not give information on the types of reactions responsible for the observed particles. Also, particle measurements were unavoidable from a certain restriction of the detection threshold ($\sim$40 MeV) of the spectrometer.

Radiochemical methods are useful for identifying individual $(\gamma,\pi^- xn)$ reactions for different x. It is possible to isolate the product nuclides chemically as a series of radioisotopes with mass numbers (A_t-x) belonging to (Z_t+1) element from a target with mass number A_t of an element with atomic number Z_t and also from the dominant spallation products of $A_p<A_t$ and $Z_p \leqslant Z_t$. The (γ,π^+) reaction leads to a product nucleus of $A_p=A_t$ and $Z_p=Z_t-1$ that is also distinguishable from those of other competitive reaction paths, though the $(\gamma,\pi^+ xn)$ products are not separable from the $(\gamma,px'n)$ products. The information obtained from the activation method is integral with respect to the energy and angle of the final products, but forgoes a detailed theoretical analysis of the final states involved [5]. However, the complete picture concerning competitive reaction paths opened by Δ resonance such as photopion reactions different in x, photospallation, photofragmentation and photofission in cases of heavy complex nuclei can be clarified. The study of the $(\gamma,\pi^- xn)$ reactions reported in this paper emphasizes the yield variations for individual x with respect to a wide range of photon energies and target compositions, A_t and $(N/Z)_t$. The (γ,π^+) yields relative to the (γ,π^-) yields over the same range of photon energies and target compositions are another concern in the present work. The results are also discussed in conjunction with a theoretical calculations based on the photon-induced intranuclear cascade analysis code (PICA) by Gabriel and Alsmiller [6,7].

II. EXPERIMENT

All of the data included in this paper were obtained from bremsstrahlung irradiations of targets (^{7}Li - ^{209}Bi) in suitable chemical forms using the 1.3 GeV Electron Synchrotron of the Institute for Nuclear Study, the University of Tokyo (now the High Energy Accelerator Research Organization, KEK, at Tanashi) in the range $E_0=250-1200$ MeV, and the 300 MeV Electron Linac of the Laboratory of Nuclear Science, Tohoku University in the range $E_0=30-270$ MeV, both using steps of 50 MeV or less. The experimental method and data analysis, including the correction method for secondary particle-induced reactions, were reported previously [1,2]. The individual procedural details, including chemical separations, will be reported elsewhere. The secondary contributions from $(p,x'n)$ reactions to $(\gamma,\pi^- xn)$ reactions on heavier targets ($A_t \geqslant 100$) were less than 10% at $E_0 \geqslant 400$ MeV, but those from (p,n) yields to (γ,π^-) yields for targets having $50 \leqslant A_t \leqslant 100$ were 20–30%, and those from the lighter targets were 40–50% (^{7}Be formation from ^{7}Li: 32%; ^{11}C formation from ^{11}B: 50%; ^{44m}Sc formation from ^{44}Ca: 13%; ^{44g}Sc formation from ^{44}Ca: 54%). The contributions of (n,p) yields to (γ,π^+) yields were about 10% for ^{65}Cu, or less than 10% for targets having $A_t>80$, but 30–55% for targets having $A_t \leqslant 60$.

In previous papers [1,2], the yields, $Y(E_0)$, were unfolded into cross sections per photon of energy k, $\sigma(k)$, after the method of Tesch [8,9] with the aid of the LOUHI-82 code [9]. It was found that the characteristic features of the target dependence for the energy-integrated cross sections, $\int_0^{E_0}\sigma(k)dk$, are the same as the measured ones,

$$Y(E_0)=\frac{\displaystyle\int_0^{E_0}\sigma(k)\cdot N(E_0,k)dk}{\displaystyle\frac{1}{E_0}\int_0^{E_0}k\cdot N(E_0,k)dk}.$$

Therefore, we present and discuss only the values of $Y(E_0)$ for some selected E_0 in this paper.

III. RESULTS AND DISCUSSION

A. Mass yield distribution

Measured (secondary-corrected) yields as a function of E_0, $Y(E_0)$ in unit of μb per equivalent quanta (μb/eq.q.), show steep rises above $E_0=140$ MeV, the photopion threshold, and attain plateaus around $E_0=300-500$ MeV, which are characteristic of the resonance process. Typical examples of the yield curves were reported previously for ^{51}V [2], ^{133}Cs [1], and ^{127}I [3] targets. The E_0-dependence of the $(\gamma,\pi^- xn)$ yields is shown in Fig. 1, where the measured yield values at $E_0=800$, 400, and 250 MeV from ^{51}V [2], ^{59}Co, ^{75}As, ^{89}Y, ^{109}Ag, ^{115}In, ^{127}I [3], ^{133}Cs [1], ^{139}La, ^{175}Lu, ^{197}Au, and ^{209}Bi targets are plotted as a function of the number of neutrons emitted (x), i.e., isotopic mass yield curves. The error bars attached to the symbols show the range of scattering in the yield curves obtained in steps of $E_0=50$ MeV or less, in the range of $E_0=30-1200$ MeV. Arrows on the symbols indicate the observed values which are not corrected for secondary contributions of less than 10%. The solid, broken, and dotted curves are drawn through the data points for $E_0=800$, 400, and 250 MeV, respectively, taking the target mass-dependent variations of all the yield values into consideration. Due to the nature of nuclear stability, most of the $(\gamma,\pi^- n)$ products are stable or long-lived and most of the $(\gamma,\pi^- 9n)$ products are too short-lived for radiochemical assays. The latter is the case for all the products from the $(\gamma,\pi^- 8n)$ reactions studied. The mass yields at $E_0=400$ and 800 MeV are almost the same and higher than those at $E_0=250$ MeV. The difference between the yield patterns for 250 MeV and 400 (and 800) MeV increases with the increasing A_t, and it becomes more promi-

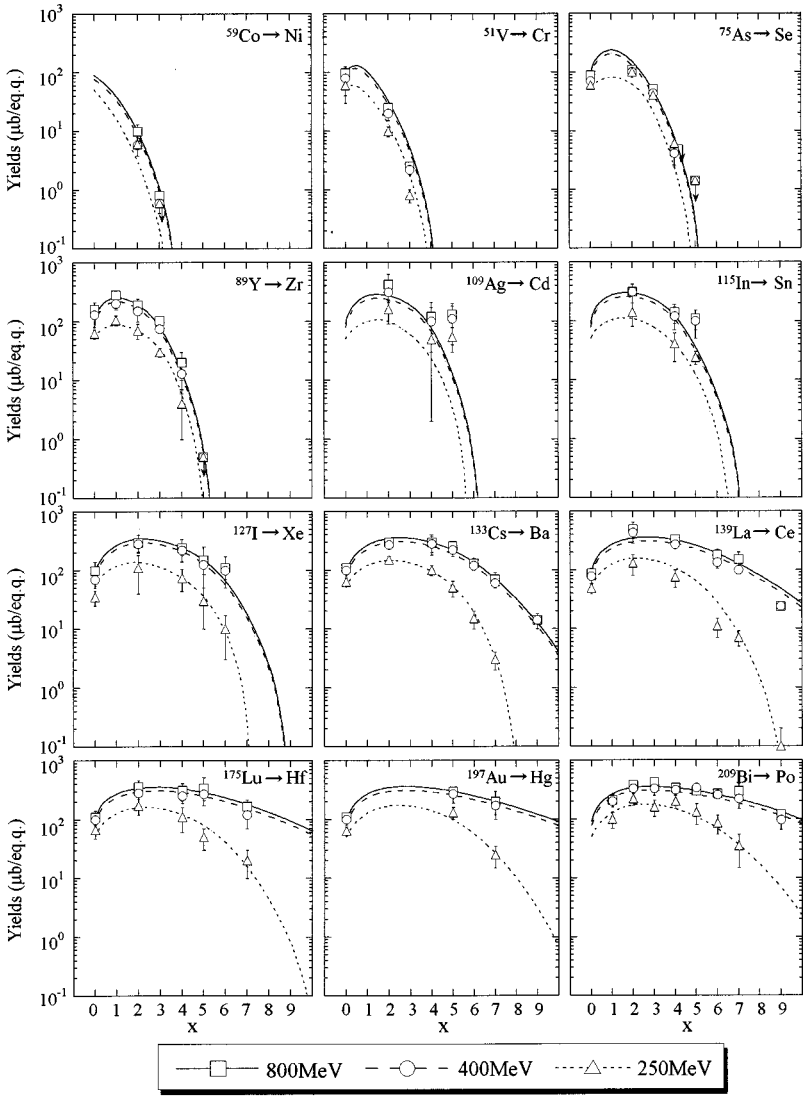

FIG. 1. Variations for $(\gamma,\pi^- xn)$ reaction yields in unit of μb per equivalent quanta (μb/eq.q.) as a function of number of emitted neutrons, x, isotopic mass yield curves, at $E_0=800$ MeV (squares connected by solid curves), 400 MeV (circles connected by broken curves), and 250 MeV (triangles connected by dotted curves).

nent at larger x in the A_t region from 127 to 209. An important feature of the isotopic mass yield curves is that the reactions of high neutron multiplicities become progressively more possible as A_t increases, and the reaction probabilities for $x=2-7$ (and even more) at $E_0\geqslant 400$ MeV are nearly comparable for a heavy target such as ^{175}Lu, ^{197}Au or ^{209}Bi, though not at $E_0=250$ MeV. On the other hand, reactions with such high neutron multiplicities are not possible for the lighter targets ($A_t\leqslant 100$). For the region of targets having $A_t=51-115$, as shown in the upper half of Fig. 1, the difference between the 250 MeV and the 400 (and 800) MeV yields is more prominent at $x=1-3$. The neutron multiplicity reflects primarily the excitation energy left after pion emission, while the energy spectrum of neutrons is to be known. Also noteworthy is that the yields for (γ,π^-) reactions are almost the same for all of the studied targets at $E_0=800$, 400, and 250 MeV.

The widths of the mass yield distributions at $E_0=400$ and 250 MeV, defined here as the x values of the $(\gamma,\pi^- xn)$ reaction for which the yield is equal to that of the (γ,π^-) reaction, 78 μb/eq.q. for $E_0=400$ MeV and 51 μb/eq.q. for $E_0=250$ MeV (see Sec. III B below), are read from the fit curves in Fig. 1 and plotted as a function of the neutron-to-proton ratio of the target, $(N/Z)_t$, in Fig. 2. The target dependence of the yields from the $(\gamma,\pi^- xn)$ reactions for $x\geqslant 1$ is not parameterized by target mass A_t, nor by the number of target neutrons N_t, because the $(\gamma,\pi^- 2n)$ and $(\gamma,\pi^- 3n)$ reaction yields from ^{51}V are higher by an order of magnitude than those from ^{59}Co, as seen in the upper left corner of Fig. 1. As noted above qualitatively, the range of neutron multiplicity is larger for heavier targets. However, the degree of the increase of the width is not monotonic, but changes largely at $(N/Z)_t=1.3-1.4$ (^{109}Ag - ^{127}I), and the rate of increase becomes smaller at $(N/Z)_t=1.32-1.35$ (^{109}Ag - ^{115}In) and at 1.49–1.52 (^{197}Au - ^{209}Bi) in the case of $E_0=400$ MeV. The change of the width at $E_0=250$ MeV is small, but the rate of increase also changes at $(N/Z)_t\fallingdotseq 1.35$. The peak positions also increase with an increase of $(N/Z)_t$ in a manner similar to the widths [see the discussion on $(\gamma,\pi^- xn)$ yields below].

B. $(\gamma,\pi^\pm)$ yields

Turning our attention to the (γ,π^-) and (γ,π^+) yields, the yield values for (γ,π^+) reactions at $E_0=800$, 400, and 250 MeV are compared with those for (γ,π^-) reactions in

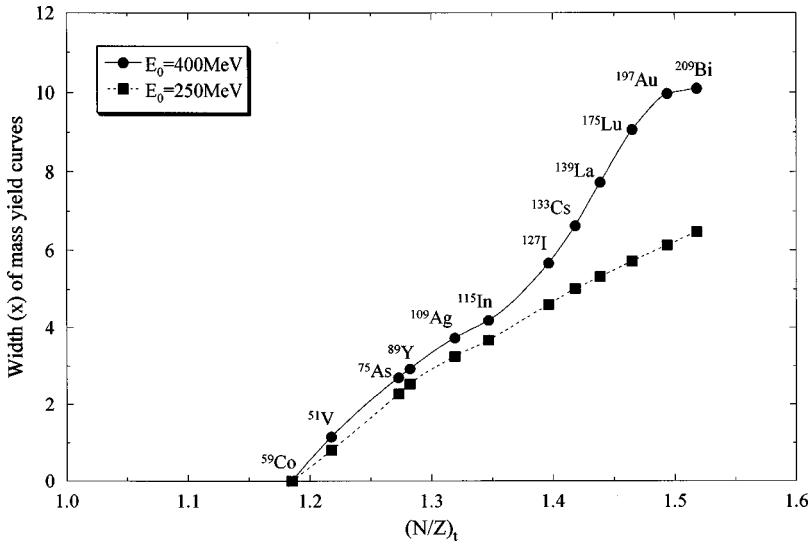

FIG. 2. Widths of the isotopic mass yield curves as a function of the neutron-to-proton ratio of the target, $(N/Z)_t$, at $E_0=400$ and 250 MeV. The width is defined as the x value of the $(\gamma,\pi^- xn)$ reaction for which the yield is equal to that of the (γ,π^-) reaction, 78 μb/eq.q. for $E_0=400$ MeV and 51 μb/eq.q. for $E_0=250$ MeV.

Figs. 3(a)–3(c), as a function of target mass A_t. Open squares represent the yields for (γ,π^+) reactions on ^{9}Be [10], ^{27}Al [11,12,13,14], ^{37}Cl, ^{41}K [13], ^{51}V [11], ^{59}Co, ^{65}Cu [13], ^{75}As, ^{87}Rb, ^{88}Sr [13], ^{109}Ag, ^{115}In, ^{133}Cs, ^{138}Ba [13], ^{139}La, and ^{181}Ta, as indicated on the lower horizontal axis of Fig. 3(b). Yield data from literature sources, except for ^{9}Be, were complemented by our own measurements over the relevant E_0 range. The $Y(E_0)$ values for the (γ,π^-) reactions are plotted as closed circles. All of the targets for (γ,π^-) reactions are indicated on the upper horizontal axis of Fig. 3(b). Literature data were used for ^{7}Li [15,16], ^{11}B [12,13,17], ^{12}C [16,18], ^{14}N [19], ^{51}V [11], ^{60}Ni [20], and ^{197}Au [21]. The large symbols show the yield values obtained by our group and the small ones the literature values by other groups. The values for the ^{14}O, ^{75}Ge, and ^{109}Pd yields from ^{14}N, ^{75}As, and ^{109}Ag, respectively, are upper limits, indicating that no corrections for the secondaries (about 10% or less for the latter two) were performed. Solid lines are the weighted means of the measured values discussed below. Dotted lines are the weighted means of the values calculated by the PICA code [6,7] for the mentioned reactions. The calculations were performed for the particle histories of $(1-4)\times10^6$ with the parameter values given previously [1,2,7]. The calculational model employed is only applicable to the reactions over the energy range of 30–400 MeV for both monoenergetic photons and thin-target bremsstrahlungs of Schiff spectra and over a range of $A_t \geqslant 12$ [6,7], so calculation at $E_0=800$ MeV is not possible.

While some of the yield values were obtained with large uncertainties, especially at $E_0=250$ MeV, both the $(\gamma,\pi^\pm)$ yields are A_t-independent except for light targets, irrespective of E_0. The yields for (γ,π^-) reactions on lighter targets such as ^{7}Li [15,16], ^{11}B [12,13,17], ^{12}C [16,18], ^{14}N [19] are anomalously small compared with those for the heavier targets. The low values for the ^{7}Be and ^{14}O yields up to $E_0=1200$ MeV were confirmed in the present work, and the low yields are explained as due to small numbers of particle stable states (two in ^{7}Be, ten in ^{11}C, one in ^{12}N and ^{14}O) [22]. Also, it is well known that the anomalously slow transition rates in the $A=14$ isobars are observed in $^{14}\mathrm{C}\rightarrow{}^{14}\mathrm{N}+e^-+\overline{\nu_e}$ and $^{14}\mathrm{O}\rightarrow{}^{14}\mathrm{N}+e^++\nu_e$ as well as in radiative pion and muon captures [13]. On the other hand, many bound states leading to (γ,π^-) reactions exist for the heavy nuclei. This manifests the A_t-independence in the heavy target region; the weighted means of the yield values of (γ,π^-) reactions on targets having $A_t \geqslant 44[^{44}\mathrm{Ca}(\gamma,\pi^-)^{44}\mathrm{Sc}]$ are 91 ± 6, 78 ± 6, and 51 ± 5 μb/eq.q. for $E_0=800$, 400, and 250 MeV, respectively (horizontal solid lines in Fig. 3). The PICA calculations for the corresponding reactions on these heavy targets at $E_0=400$ MeV are smaller than the measured values by 35% on average, though the calculations also indicate A_t-independence. The same trend holds at $E_0=250$ MeV.

The (γ,π^+) reaction yields are also A_t-independent for $A_t \geqslant 27[^{27}\mathrm{Al}(\gamma,\pi^+)^{27}\mathrm{Mg}]$, and their weighted means are 18 ± 2, 14 ± 2, and 7.3 ± 1.1 μb/eq.q. for $E_0=800$, 400, and 250 MeV, respectively. A large number of yield measurements for ^{27}Mg from $^{27}\mathrm{Al}(\gamma,\pi^+)$ reaction have been reported, but the results are quite different among the different reports. The present results fall in between those of Masaike [14] and of Blomqvist *et al.* [13]. The values of Noga *et al.* [12] and of the present work seem to be consistent with the mean values obtained from the heavier targets. The yield values reported for $^{9}\mathrm{Be}(\gamma,\pi^+)^{9}\mathrm{Li}$ in the energy range of $E_0=100-800$ MeV by Nilsson *et al.* [10] are definitely smaller than the trend, probably because there are only two bound states in ^{9}Li. Although both the (γ,π^+) and (γ,π^-) reactions on the light nuclei have been of interest from a theoretical point of view [5], they are not included in our discussions with those of the heavier complex nuclei which allow for statistical treatments. The PICA calculation for (γ,π^+) reactions in the heavy target region also reproduces the A_t-independence, but the average values obtained from the calculations are two times those of the measurements. Thus, the measured yields in the A_t-independent region at $E_0=400$ and 800 MeV give a yield ratio of $Y(\gamma,\pi^-)/Y(\gamma,\pi^+)=5.6\pm1.0$, while the corresponding PICA value at $E_0=400$ MeV is 1.8 ± 0.3, confirming the previous findings discussed above. At $E_0=250$ MeV, the experimental $Y(\gamma,\pi^-)/Y(\gamma,\pi^+)$ ratio is 7.0 ± 1.3 and the calculated one is 2.2 ± 0.3, both of which are somewhat larger than the corresponding ones at $E_0=400$ MeV, though almost within the error limits. It is noted, however, that the excitation curve, $\sigma(k)$, obtained from unfolding of the $Y(E_0)$

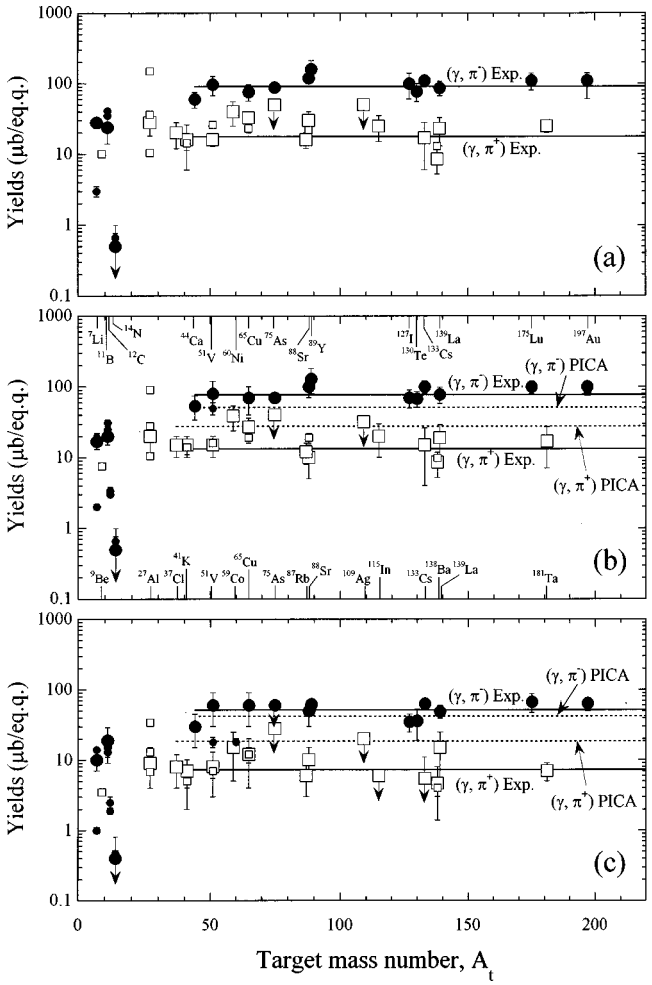

FIG. 3. Target mass dependence of the $(\gamma,\pi^{\pm})$ yields in unit of μb per equivalent quanta (μb/eq.q.) at $E_0=800$ MeV (a), $E_0=400$ MeV (b), and $E_0=250$ MeV (c). Closed circles represent the (γ,π^-) yields and open squares the (γ,π^+) yields. The large symbols show the values obtained by the author's group and the small ones from the literature (see text), as measured for the targets indicated along the upper axis for the (γ,π^-) reactions and the lower axis for the (γ,π^+) reactions in (b). The arrow symbols show measured values not corrected for secondary contributions. The solid lines are the weighted means of $Y(E_0)$ for (γ,π^-) reactions on targets with $A_t\geqslant 44$ and for (γ,π^+) reactions on $A_t\geqslant 27$. The dotted lines in (b) and (c) show the average PICA results calculated for the same reactions.

curve, peaks around $k=200$ MeV for the (γ,π^-) reaction and almost vanishes above 300 MeV. The $\sigma(k)$ curve for the (γ,π^+) reaction peaks around $k=230$ MeV and levels off to vanishing values above 350 MeV (see examples in Refs. [1] and [2]). Because of this difference, the experimental $Y(E_0)$ values for the (γ,π^+) reactions around $E_0=250$ MeV increase more rapidly with an increase of E_0 compared with the corresponding ones for the (γ,π^-) reactions. The $Y(E_0)$ ratio also tends to be higher compared to those at higher E_0. The reason for the difference in the peak energies for the two types of reactions is not clear, though the phase space felt by π^- and π^+ may differ as observed in $\beta^{\pm}$ emissions. It is noted that the PICA calculations produce the same peak energies for the excitation curves for both $(\gamma,\pi^{\pm})$ reactions.

The high observed yield ratios compared with the calculated ones may imply new nuclear structure effects that are not taken into consideration in the theoretical foundation of the PICA code. The nuclear model used in the theoretical calculations is exactly the same as the one used in the Bertini calculations [23]. The continuous charge density distribution inside the nucleus, $\rho(r)=\rho_0/\{1+\exp[(r-c)/z_1]\}$, c and z_1 being the relevant parameters, obtained by electron scattering data [24], was approximated by dividing the nucleus into three concentric spheres: a central sphere and two surrounding spherical annuli having the uniform densities of 0.9, 0.2, and 0.01 of $\rho(0)$ at the center of the nucleus. The neutron to proton density ratios were assumed to be equal to the ratio of neutrons to protons for the entire nucleus. Cross sections for the photoabsorption by a nucleon in the (3, 3) resonance region were taken from those for elementary processes for free nucleon-photon interactions, by assuming $\sigma(\gamma p\rightarrow n\pi^+)=\sigma(\gamma n\rightarrow p\pi^-)$ from charge-symmetry considerations. And the intranuclear cascade calculation of Bertini [24] was then used to account for the secondary effect of nucleon- and pion-interactions with the remaining nucleus following the initial photon interaction. Pion absorption is assumed to occur via a two-nucleon mechanism with a cross section for the absorption of a charged pion by a nucleon with isobaric spin projection of the opposite sign (i.e., a pair of nucleons must contain at least one proton to absorb a negative pion and at least one neutron to absorb a positive pion).

The higher yields of the (γ,π^-) reactions and the lower ones of the (γ,π^+) reactions relative to those expected from the PICA calculation could possibly be understood if the neutron density in nuclear surface region is higher than the inner density of the nucleus. An initial production of negative pions by way of $\gamma+n\rightarrow\Delta^0\rightarrow p+\pi^-$ would be more probable than those of positive pions by way of $\gamma+p\rightarrow\Delta^+\rightarrow n+\pi^+$, and the secondary absorption of negative pions by way of π^-+pp or π^-+pn would be less than those for positive pions by way of π^++np or π^++nn in the neutron-rich surface region.

These processes which lead to (γ,π^-) and (γ,π^+) reactions are, therefore, considered here to occur in the surface region of the nucleus, but experimental observations seem to show that the cross sections are not proportional to $A_t^{2/3}$ but A_t-independent. This A_t-independence may be explained as due to a compensation for the increase in pion production with increasing nuclear size (surface) by the competitive increase of neutron emissivity associated with pion emission (see Sec. III C). The available final transitions are, therefore, limited to a certain number of levels below the particle separation energy which is set equal to 7 MeV in PICA. While the number of the bound states and the strength of transitions to these states are unknown, they must be statistically significant, as the A_t-independence from the PICA calculation also suggests. There has been no evidence for the density difference between protons and neutrons in the stable nucleus, but neutron skin and neutron halo structures have been discovered in very neutron-rich light nuclei near the drip line [25]. Further study of structural changes in nuclei closer to the stability line is required; the present work suggests photonuclear processes may cause such effects.

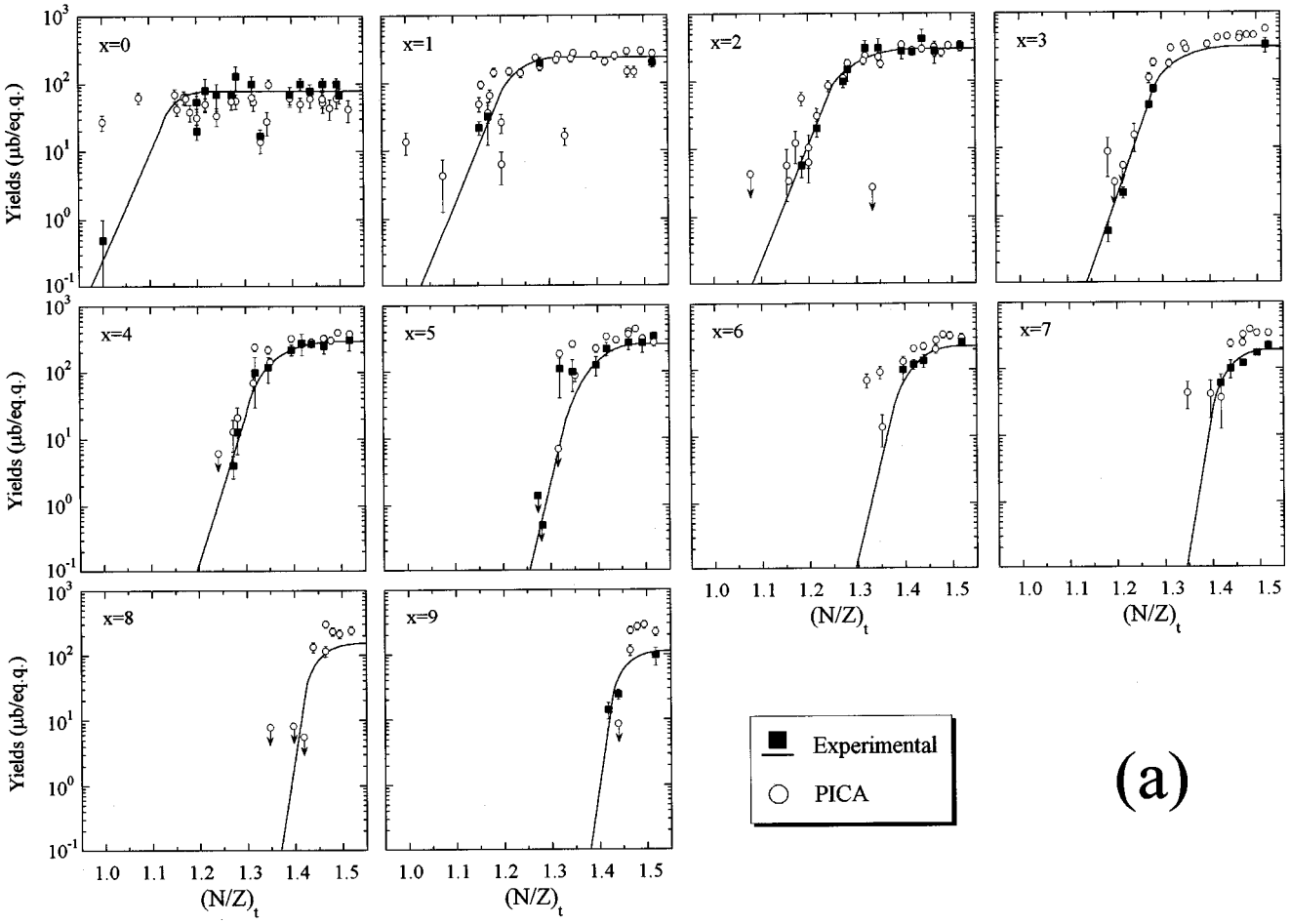

FIG. 4. Variations in the $(\gamma,\pi^- xn)$ reaction yields in unit of μb per equivalent quanta (μb/eq.q.) for $x=0-9$ as a function of the proton-to-neutron ratio of target, $(N/Z)_t$, at $E_0=400$ MeV (a) and 250 MeV (b). Experimental values are shown as closed squares, and PICA calculations are shown as open circles.

C. $(\gamma,\pi^- xn)$ yields

In order to reveal the target-dependent changes of the $(\gamma,\pi^- xn)$ reaction yields for each x of $x\geqslant 0$, the yield values at $E_0=400$ and 250 MeV (closed squares) are plotted in Figs. 4(a) and 4(b) as a function of the neutron-to-proton ratio of the entire target nucleus, $(N/Z)_t$. Solid lines representing $x=0-9$ are drawn through the observed points with the aid of the smoothed mass yield curves in Fig. 1. Also plotted in Fig. 4 are the yield values calculated for $E_0=400$ and 250 MeV (open circles) by the PICA code [7].

The yield values change systematically with respect to x and $(N/Z)_t$. Both the observed and the calculated values for the individual reactions begin at a certain $(N/Z)_t$, increase rapidly with increasing $(N/Z)_t$, and reach a plateau at $E_0=400$ MeV [Fig. 4(a)]. At $E_0=250$ MeV [Fig. 4(b)], the increase in the reaction yields for $x\geqslant 4$ slows and does not reach a clear plateau. The features at $E_0=250$ MeV are a reflection of the excitation functions for these reactions; the threshold and peak energies of the excitation functions increase almost exponentially with increasing x, the reactions for $x\leqslant 4$ have peaks at photon energies of $k\leqslant 250$ MeV, and cross sections for the $(\gamma,\pi^- 9n)$ reaction nearly vanish above $k\geqslant 400$ MeV [1,2]. The PICA calculations approximate the observed profiles as a whole. Notably, the positive slope regions of the $Y(E_0)$ vs $(N/Z)_t$ curves are well reproduced, with some exceptions at $(N/Z)_t=1.18(^{59}\mathrm{Co})$, $1.32(^{109}\mathrm{Ag})$, and $1.35(^{115}\mathrm{In})$, whereas the plateau values are largely discrepant. The PICA results underestimate by 35% the (γ,π^-) yields as noted above, but increasingly overestimate by factors of 1.5–2.0 the $(\gamma,\pi^- xn)$ reaction yields for $x\geqslant 3$. The deviation increases with the increasing x. The calculations for light targets such as ^{7}Li, ^{11}B, ^{12}C, ^{14}N and ^{27}Al, for which observed values for either the (γ,π^-) or (γ,π^+) reactions are available, show small yields for reactions with $x=1-2$, and show large deviations from the smooth trends of the yields for the heavier targets.

The sums of the $(\gamma,\pi^- xn)$ yields at $E_0=400$ and 250 MeV are shown in Figs. 5(a) and 5(b), respectively. In the figures, the sums of the measured yields of the reactions of $x=0$ to $1,2,\ldots,9$ and the maximum possible x (max), $\Sigma_{i=0}^{x} Y_i(N/Z)_t$, are shown as solid lines. The two dotted curves indicate the range of values for the total yield, $\Sigma_{i=0}^{\max} Y_i(N/Z)_t$, as calculated by PICA. The total of the measured yields increases sigmoidally with increasing $(N/Z)_t$; a close inspection reveals that the total yield curve consists of two sigmoids, one from $(N/Z)_t=1.01$ to 1.35 and the other from $(N/Z)_t=1.35$ to 1.55. The second steep sigmoid is the reflection of the rapid increase in the $(\gamma,\pi^- xn)$ yields for $x\geqslant 5$ for targets with $(N/Z)_t\geqslant 1.35$, which is consistent with the change in the width of the mass yield curves shown in Fig. 2. At $E_0=250$ MeV, there are no significant contributions from reactions with $x\geqslant 8$ to the total yield, and the

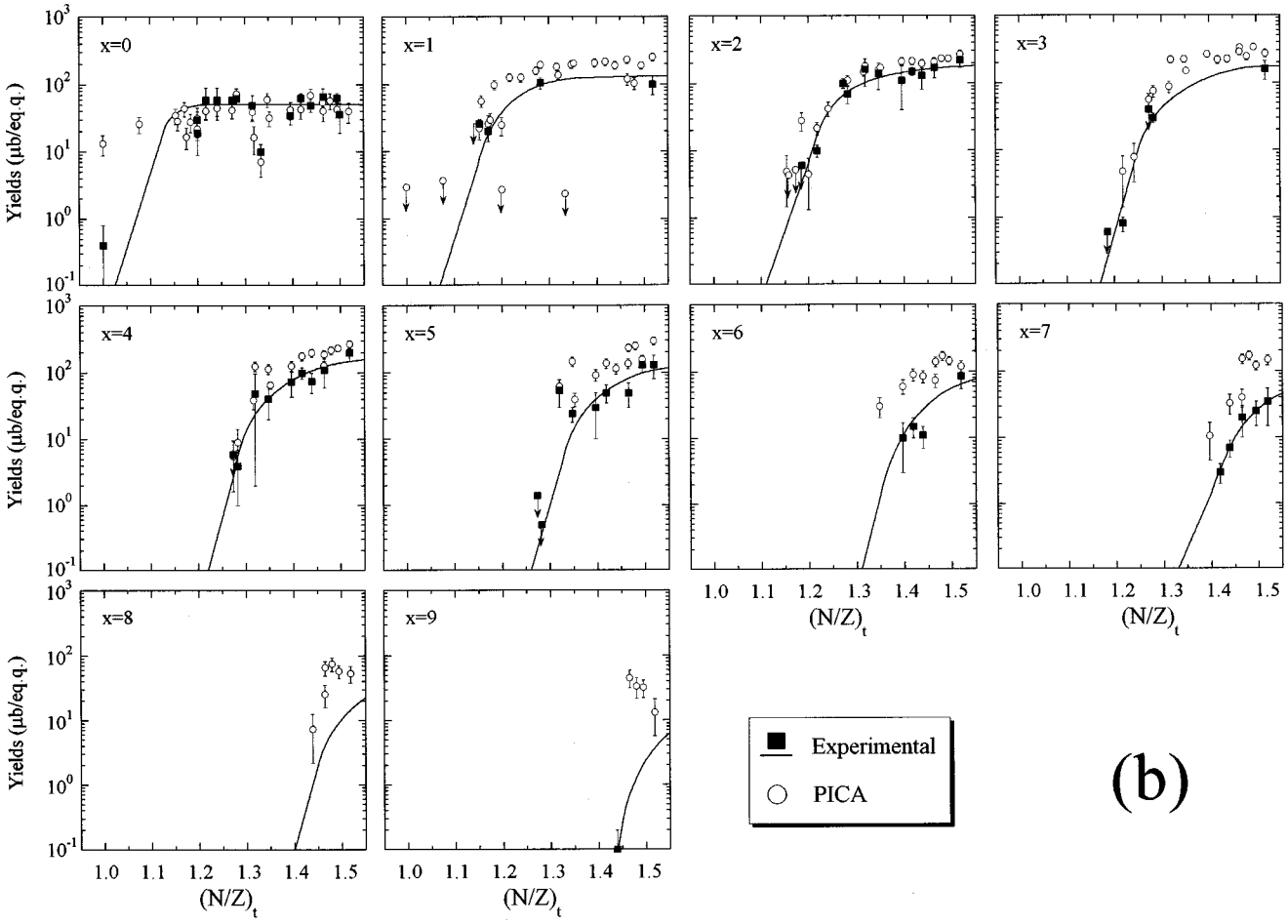

FIG. 4. *(Continued).*

existence of two sigmoids is not very clear due to the reasons described above for the excitation functions. The PICA results for the $\Sigma_{i=0}^{\max} Y_i(N/Z)_t$ fall in the region between the two dotted curves at $E_0=400$ and 250 MeV.

The fact that the variations in the observed reaction yields are well parameterized with $(N/Z)_t$, but not with A_t or N_t, suggests that photopion reactions are initiated by competitive photoabsorptions by neutrons and protons in the entire nucleus. Also, the rapid but sigmoidal increase of the total (final) yields with increasing $(N/Z)_t$ does not appear to conflict with the nuclear model of neutron-rich surface proposed earlier. The richer the concentration of neutrons in the outer region of the nuclei, the smaller the amount of negative-pion reabsorption, and also the more probable the occurrence of multiple-neutron-emission. For $(\gamma,\pi^- xn)$ reactions with $x\geqslant 1$, pions may carry small amounts of kinetic energy which allow emission of multiple neutrons during both the cascade process and the evaporation process from the excited cascade residue. The latter would be dominant in $(\gamma,\pi^- xn)$ reactions of large x which are possible in target nuclei of larger $(N/Z)_t$. The energies of the emitted particles may be too low to be detected by current spectrometers, and this target-dependence difference from particle measurements could be explained by differences noted in the radiochemical observations.

In order to characterize the features of $Y(E_0)$ vs $(N/Z)_t$ more quantitatively, the ''target thresholds,'' $(N/Z)_{th}$, the slopes of the rising portions of the curves and the values at the plateau at $E_0=400$ MeV are plotted as a function of x in Figs. 6(a)–6(c). The ''target threshold'' is defined here as that $(N/Z)_t$ for which each $(\gamma,\pi^- xn)$ reaction starts to occur with a certain probability, say 1 μb/eq.q. It is shown to increase linearly with increasing x from 0 to 5. This linear section can be described by $(N/Z)_{th}=1.040+0.050x$ at $E_0=400$ MeV and also at $E_0=800$ MeV. At $E_0=250$ MeV, $(N/Z)_{th}=1.100+0.046x$. Also plotted in Fig. 6(a) are the $(N/Z)_{th}$ for the yields at 5, 10, 50, 100, 150, 250, and 300 μb/eq.q. A group of the linear arrays is shown to exist over shorter ranges of x. These relationships can be used to predict the unmeasured yields of those reactions. Some deviations from a linear relationship occur at $x>5$ for the 1 μb/eq.q. threshold and also for the thresholds of the larger yields, suggesting that there may be some change in the reaction process in the heavy target region of $(N/Z)_t$ corresponding to $(N/Z)_{th}\geqslant 1.3-1.4$, where reactions involving high neutron multiplicities can occur. The slopes for the rapidly rising yield section for individual reactions with respect to $(N/Z)_t$ are almost the same for $x=0-2$, but then increase especially for $x\geqslant 5$ [Fig. 6(b)]. The maximum yields decrease very slowly with increasing x from 300 μb/eq.q. at $x=3$ to 100 μb/eq.q. at $x=9$ [Fig. 6(c)]. Also shown in Fig. 6(c) are the results of the PICA calculations (open circles). The fact that the PICA code underestimates the (γ,π^-) yield by 35% and overestimates the $(\gamma,\pi^- xn)$ yields for $x\geqslant 3$ by a factor of about 2, as noted above, is clearly demonstrated.

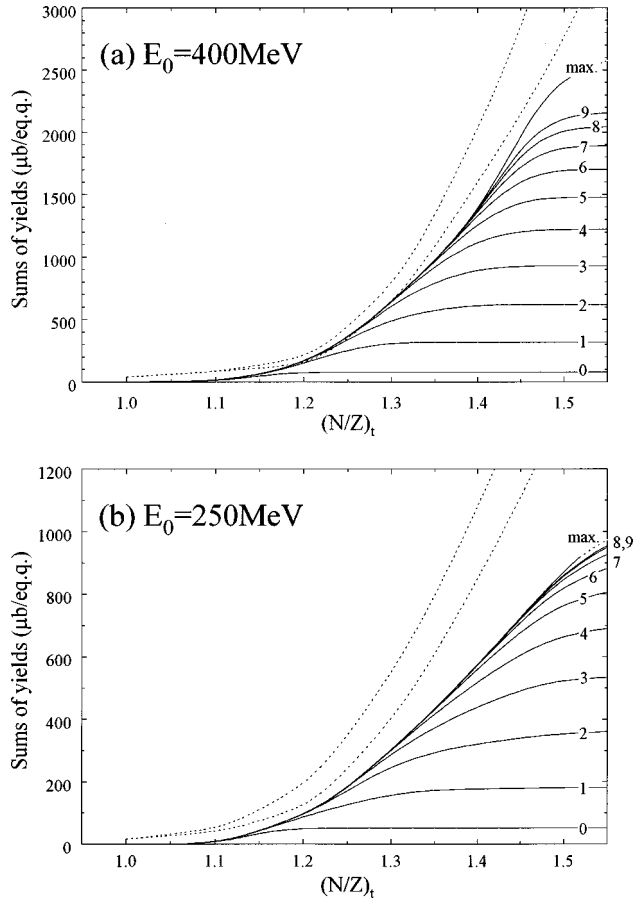

FIG. 5. The sum of the $(\gamma,\pi^- xn)$ yields, $\Sigma_{i=0}^{x} Y_i(N/Z)_t$, in unit of μb per equivalent quanta (μb/eq.q.). Solid lines are the sums of the measured yields, $Y_i(N/Z)_t$ from Fig. 4 for $x=0$ to $x=1,2,\ldots,$ maximum possible x (max). Dotted curves show the range of the total yields obtained from the PICA calculations. (a) for $E_0=400$ MeV and (b) for $E_0=250$ MeV.

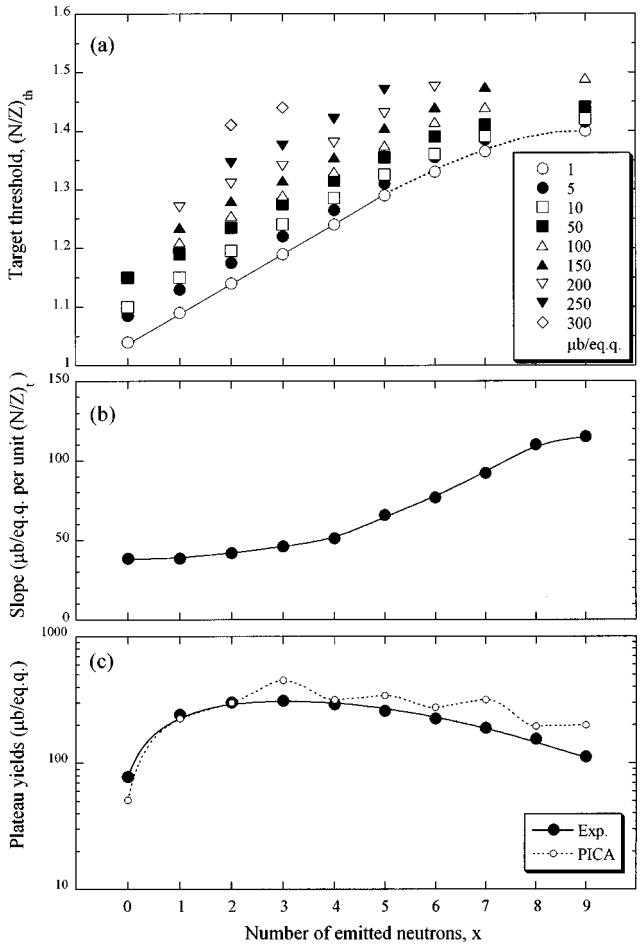

FIG. 6. Characteristics of the $(\gamma,\pi^- xn)$ yield profiles at $E_0=400$ MeV. (a) Variations in the ''target threshold $(N/Z)_{th}$'' for the yields of 1, 5, 10, 50,...,300 μb per equivalent quanta (μb/eq.q.) as a function of x at $E_0=400$ MeV [see text for definition of $(N/Z)_{th}$]. (b) Slopes of the rising yield sections for the individual reactions, μb/eq.q. per unit $(N/Z)_t$, as a function of x. (c) Maximum yields of the individual $(\gamma,\pi^- xn)$ reactions for different x as a function of x. Closed circles connected with a solid line denote the measured yields and open circles connected by dotted line denote the PICA calculated yields.

Also the PICA yields show a zigzag pattern due to an even-odd effect [1]. The overestimations for the plateau values for $x\geqslant 3$ by the PICA code are due to higher cross sections (lower transparencies) for emission of negative pions and neutrons than are required. In our study of photo-spallation of the type such as $(\gamma,xnyp)$ over a wide range of target nuclei [26] similar to the present work, the PICA calculations were found to overestimate the spallation yields of large $(x+y)$ especially for heavier targets.

The existence of plateaus in the yields for $(\gamma,\pi^- xn)$ reactions of individual x might be due to the increase of multineutron emission of larger x being compensated by an increase in nuclear size. Unfortunately, radiochemical methods can not distinguish the $(\gamma,\pi^+ xn)$ yields from the more dominant $(\gamma,px'n)$ yields for $x=x'-1\geqslant 1$ because the product nuclides from both reactions are the same.

All of the facts point to changes in the widths of the isotopic mass yield curves, the ''target thresholds'' $(N/Z)_{th}$, the slopes in the sections of increasing yields with respect to $(N/Z)_t$, and the maximum yields at $(N/Z)_t=1.3-1.4$, above which the occurrence for $(\gamma,\pi^- xn)$ reactions of $x\geqslant 5$ become pronounced. It is suggested that changes in the yield profiles for targets heavier than $A_t=100$ might be associated with pronounced nuclear medium effects giving rise to more excessive excitation as compared with medium-heavy targets $(A_t\leqslant 100)$.

A more advanced theoretical model concordant with the present findings needs to be developed in order to better quantify the results.

ACKNOWLEDGMENTS

The authors are indebted to Dr. M. Yagi, Dr. K. Masumoto, Dr. T. Ohtsuki and the linac crew members of the Laboratory of Nuclear Science, Tohoku University, and Dr. K. Yoshida, Dr. H. Okuno, Dr. K. Maruyama, Dr. M. Imamura and the ES crew members of the Institute for Nuclear Study, University of Tokyo, for their invaluable assistance regarding in accelerator operations, and to the former students of the Radiochemistry Laboratory of Kanazawa University for radiochemical experiments. This work was supported by a Grant-in-Aid for Scientific Research (01470049 and 07304077) of the Ministry of Education, Science and Culture of Japan.

[1] K. Sakamoto, Y. Hamajima, M. Soto, Y. Kubota, M. Yoshida, A. Kunugise, M. Masatani, S. Shibata, M. Imamura, M. Furukawa, and I. Fujiwara, Phys. Rev. C **42**, 1545 (1990).
[2] K. Sakamoto, M. Yoshida, Y. Kubota, T. Fukasawa, A. Kunugise, Y. Hamajima, S. Shibata, and I. Fujiwara, Nucl. Phys. **A501**, 693 (1989).
[3] Y. Oura, A. Yazawa, M. Yoshida, S. R. Sarkar, K. Sakamoto, S. Shibata, I. Fujiwara, and M. Furukawa, Radiochim. Acta **68**, 27 (1995).
[4] J. Arends, P. Detemple, N. Floss, S. Huthmacher, G. Kaul, B. Mecking, G. Nöldeke, and R. Stenz, Nucl. Phys. **A526**, 479 (1991).
[5] A. Nagl, V. Devanathan, and H. Überall, *Nuclear Pion Photoproduction* (Springer-Verlag, Berlin, 1991).
[6] T. A. Gabriel and R. G. Alsmiller, Jr., Phys. Rev. **182**, 1035 (1969).
[7] T. A. Gabriel, M. P. Guthrie, and O. W. Hermann, Oak Ridge National Laboratory Report No. ORNL-4687 (1971).
[8] K. Tesch, Nucl. Instrum. Methods **95**, 245 (1971).
[9] J. T. Routti and J. V. Sandberg, Comput. Phys. Commun. **21**, 119 (1980).
[10] M. Nilsson, B. Schröder, B. Bülow, J. Grintals, G. G. Jonsson, B. Lindner, K. Srinivasa Rao, and S. Susila, Z. Phys. A **294**, 253 (1980).
[11] I. Blomqvist, P. Janeček, G. G. Jonsson, H. Dinter, K. Tesch, N. Freed, and P. Ostrander, Phys. Rev. C **15**, 988 (1977).
[12] V. I. Noga, Yu. N. Ranyuk, P. V. Sorokin, and V. A. Tkachenko, Sov. J. Nucl. Phys. **14**, 506 (1972).
[13] I. Blomqvist, G. Nydahl, and B. Forkman, Nucl. Phys. **A162**, 193 (1971).
[14] A. Masaike, J. Phys. Soc. Jpn. **19**, 427 (1964).
[15] V. I. Noga, Yu. N. Ranyuk, P. V. Sorokin, and V. A. Tkachenko, Ukr. Phys. J. **16**, 1850 (1971) (in Russian).
[16] P. E. Bosted, K. I. Blomqvist, and A. M. Bernstein, Phys. Rev. Lett. **43**, 1473 (1979).
[17] I. S. Hughes and P. V. March, Proc. Phys. Soc. London **72**, 259 (1958).
[18] V. D. Epaneshnikov, V. M. Kuznetsov, and O. I. Stukov, Sov. J. Nucl. Phys. **19**, 242 (1974).
[19] V. DeCarlo, N. Freed, W. Rhodes, B. Bülow, G. G. Jonsson, K. Lindgren, and R. Pettersson, Phys. Rev. C **21**, 1460 (1980).
[20] P. V. March and T. G. Walker, Proc. Phys. Soc. London **77**, 293 (1960).
[21] I. Blomqvist, B. Bülow, A. Fredrikson, B. Johnsson, G. G. Jonsson, K. Lindgren, M. Nilsson, R. Petersson, O. Glomset, N. Freed, and W. Rhodes, Z. Phys. A **288**, 313 (1978).
[22] Y. Oura, K. Kawaguchi, S. R. Sarkar, H. Haba, Y. Miyamoto, K. Sakamoto, S. Shibata, I. Fujiwara, and M. Furukawa, Research Report of Laboratory of Nuclear Science, Tohoku University **27**, 133 (1994).
[23] H. W. Bertini, Phys. Rev. **131**, 1801 (1963).
[24] R. Hofstadter, Rev. Mod. Phys. **28**, 214 (1956).
[25] P. G. Hansen, A. S. Jensen, and B. Jonson, Annu. Rev. Nucl. Part. Sci. **45**, 591 (1995); I. Tanihata, J. Phys. G **22**, 157 (1996).
[26] S. R. Sarkar, Y. Oura, K. Kawaguchi, A. Yazawa, K. Sakamoto, S. Shibata, and I. Fujiwara, Radiochim. Acta **62**, 7 (1993).